Random migration precedes stable target cell interactions of tumor-infiltrating T cells

Paulus Mrass,[1] Hajime Takano,[2] Lai Guan Ng,[1] Sachin Daxini,[1] Marcio O. Lasaro,[1] Amaya Iparraguirre,[1] Lois L. Cavanagh,[1] Ulrich H. von Andrian,[5] Hildegund C.J. Ertl,[1] Philip G. Haydon,[2] and Wolfgang Weninger[1,3,4]

[1]Immunology Program, The Wistar Institute, Philadelphia, PA 19104
[2]Department of Neuroscience and Conte Center for Integration at the Tripartite Synapse, [3]Department of Dermatology, and [4]Department of Pathology and Laboratory Medicine, University of Pennsylvania School of Medicine, Philadelphia, PA 19104
[5]CBR Institute for Biomedical Research and Department of Pathology, Harvard Medical School, Boston, MA 02215

The tumor microenvironment is composed of an intricate mixture of tumor and host-derived cells that engage in a continuous interplay. T cells are particularly important in this context as they may recognize tumor-associated antigens and induce tumor regression. However, the precise identity of cells targeted by tumor-infiltrating T lymphocytes (TILs) as well as the kinetics and anatomy of TIL–target cell interactions within tumors are incompletely understood. Furthermore, the spatiotemporal conditions of TIL locomotion through the tumor stroma, as a prerequisite for establishing contact with target cells, have not been analyzed. These shortcomings limit the rational design of immunotherapeutic strategies that aim to overcome tumor–immune evasion. We have used two-photon microscopy to determine, in a dynamic manner, the requirements leading to tumor regression by TILs. Key observations were that TILs migrated randomly throughout the tumor microenvironment and that, in the absence of cognate antigen, they were incapable of sustaining active migration. Furthermore, TILs in regressing tumors formed long-lasting (≥30 min), cognate antigen–dependent contacts with tumor cells. Finally, TILs physically interacted with macrophages, suggesting tumor antigen cross-presentation by these cells. Our results demonstrate that recognition of cognate antigen within tumors is a critical determinant of optimal TIL migration and target cell interactions, and argue against TIL guidance by long-range chemokine gradients.

CORRESPONDENCE
Wolfgang Weninger:
weninger@wistar.org

Abbreviations used: ECFP, enhanced cyan fluorescent protein; ECM, extracellular matrix; EYFP, enhanced yellow fluorescent protein; PLN, peripheral LN; TIL, tumor-infiltrating T lymphocyte.

T cells have the capacity to induce tumor regression, which provides the rationale for their exploitation in the therapy of cancer (1–9). To execute their antitumor activities, it is thought that T cells need to physically engage target cells within the tumor microenvironment, which results in the recognition of tumor-associated antigens in the context of MHC class I or II molecules. As a prerequisite, T cells must home to tumor sites via the blood stream, and then traverse the interstitial space to eventually reach their targets. Besides tumor cells, the tumor microenvironment harbors a variety of host-derived cells, such as endothelial cells, fibroblasts, innate and adaptive immune cells, as well as extracellular matrix (ECM) fibers, cytokines, and other mediators. All of these components may be involved in shaping the migratory and interactive behavior of tumor-infiltrating T lymphocytes (TILs).

Although recent advances in noninvasive imaging approaches, such as bioluminescence and magnetic resonance imaging, have made possible longitudinal studies of the trafficking of effector T cells into tumors at the population level (10, 11), the precise behavior of TILs at the single cell level within the three-dimensional context of the tumor microenvironment is unknown. Thus, fundamental questions regarding the critical final steps of tumor immunity have remained unanswered. For example, it has been speculated that T cells follow chemotactic gradients within inflammatory sites, including the tumor microenvironment, implying directed migration at the population level (12–15). However, this hypothesis has

The online version of this article contains supplemental material.

The Journal of Experimental Medicine

not been tested within intact tumors. In addition, we do not know the exact identity of cells targeted by TILs. Although tumor cells are likely candidates, TILs may also interact with stromal cells, such as macrophages and dendritic cells, cross-presenting tumor-associated antigens (16). Interactions with stromal cells may not only be important for the activation of TILs within tumors leading, for example, to cytokine production, but may also directly contribute to tumor regression through stromal cell destruction (17). Finally, the dynamics of TIL-target cell interactions have not been studied. Although in vitro studies have shown that T cells undergo long-term, cognate antigen–dependent interactions with tumor cells (18–20), cellular behavior in vivo may follow different rules. Thus, although it is not known whether TIL-target cell interactions are short- or long-lived, the duration of interactions may be important for the formation of the immunologic synapse. A detailed understanding of these open questions at the cellular and molecular level may help to optimize therapeutic regimens, as T cell responses could be manipulated to increase therapeutic efficacy.

In this study we investigated the behavior of TILs using two-photon microscopy (21–34) in combination with a transgenic mouse strain, DPE^{GFP}, in which T cells express the GFP. We found that TILs migrated randomly before engaging directly with tumor cells and macrophages. Furthermore, cognate antigen at the target site was an important regulatory element of the migration and interaction of TILs.

RESULTS

Migratory behavior of endogenous naive T cells within LNs

Thus far, two-photon imaging of T cell immune responses has been exclusively performed with adoptively transferred antigen-specific T cells. We have recently developed a transgenic mouse strain, DPE^{GFP}, with GFP expression in all T cells. In these mice, GFP is driven under the control of the distal and proximal CD4 enhancers and CD4 promoter (35, 36). The construct lacks a silencer element that silences CD4 expression in mature CD8$^+$ T cells; consequently, the transgene is expressed in both CD4$^+$ and CD8$^+$ T cells (35). Flow cytometry revealed that GFP was expressed by ~98% of CD3$^+$ T cells in the peripheral LNs (PLNs) of DPE^{GFP} mice (Fig. 1 a). The high level of GFP expression was further corroborated by immunofluorescence staining of PLN sections, which showed large numbers of GFP$^+$ cells

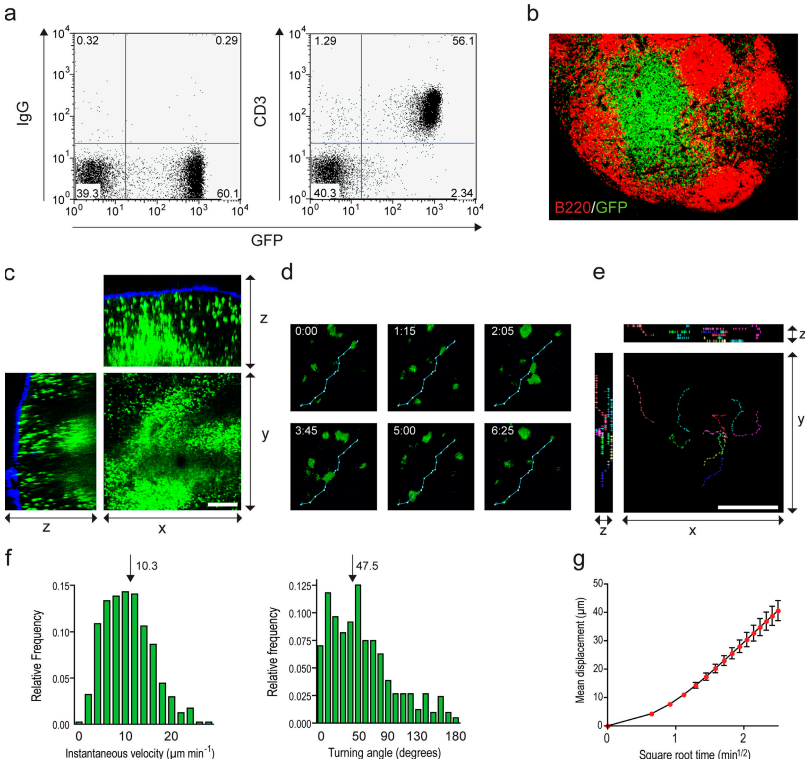

Figure 1. Migratory behavior of endogenous T cells within explanted PLNs. (a) Single cell suspensions of pooled PLNs from 4-mo-old DPE^{GFP} mice were stained using isotype control or anti-CD3 mAbs. Gates were set on viable cells. (b) Frozen sections of a DPE^{GFP} PLN were immunostained for B220 (red). (c) An inguinal LN from a DPE^{GFP} mouse was explanted, and GFP$^+$ cells were visualized by two-photon microscopy as described in Materials and methods, with the exception that x-y planes were 584 by 584 μm (resolution, 1.14 μm pixel^{-1}) and the step size was 4 μm. GFP$^+$ T cells (green) were covisualized with ECM fibers (second harmonic generation; blue). Bar, 100 μm. (d) A representative track of a migrating T cell is shown. The numbers indicate minutes/seconds. (e) Representative tracks of an analyzed region are shown. Bar, 100 μm. (f) The instantaneous velocities and turning angles of the T cell tracks were calculated. The relative frequencies of these parameters are charted. The arrows indicate the median values of each measurement. (g) The mean displacement is charted versus the square root of time.

in the paracortical regions, but not in B cell follicles (Fig. 1 b). Collectively, these results show that the DPE^{GFP} mouse strain enables visualization of endogenous T cells without the need for adoptive transfer, which has the distinct advantage that immune responses can be studied under more physiologic conditions.

To set up our imaging model and compare the migratory behavior of endogenous polyclonal naive T cells with that published for TCR transgenic T cells, we performed imaging experiments in intact explanted PLNs under conditions maintaining tissue viability (28). Fig. 1 c and Videos S1 and S2 (available at http://www.jem.org/cgi/content/full/jem.20060710/DC1) show that by two-photon imaging, GFP$^+$ cells were clearly detectable deep within the intact PLN, up to 300 μm below the capsule. The migratory behavior of GFP$^+$ cells was then analyzed by single cell tracking (see Materials and methods; Fig. 1, d and e, and Videos S1 and S2). Consistent with previous reports, naive T cells migrated at a median velocity of 10.3 μm min^{-1} and with a median turning angle of 47.5° (Fig. 1 f). The linear relationship between mean displacement of tracked cells and the square root of time indicated that polyclonal T cells migrated randomly (Fig. 1 g). Collectively, these data show that GFP$^+$ T cells in DPE^{GFP} mice behaved according to published parameters (28–30).

TILs migrate randomly within the tumor microenvironment

To analyze the migratory and interactive behavior of TILs, we implanted TC-1 lung epithelial tumor cells subcutaneously into the flanks of DPE^{GFP} mice. TC-1 cells are transformed by the human papilloma virus-16 E6/E7 as well as c-Ha-ras oncogenes. Vaccination of mice with a replication-defective E1/E3-deleted adenovirus human strain 5 expressing E7 protein induced E7-specific effector T cells that lyse E7-presenting cells (37) and cause rejection of TC-1 tumors (Fig. 2 a). In the absence of vaccination or when using a control vector expressing an unrelated protein, the tumors continued to grow exponentially (38 and not depicted). E7-MHC class I tetramer staining highlighted the influx of antigen-specific T cells into the tumors in a time-dependent manner (Fig. 2 b), and histology of TC-1 tumors illustrated that GFP$^+$ cells were distributed diffusely throughout the tumor tissues and interspersed between tumor cells (Fig. 2 c). Although there was a clear difference in the absolute number of TILs in control and vaccinated mice, their activation status (Fig. S1, available at http://www.jem.org/cgi/content/full/jem.20060710/DC1) as well as their size (not depicted) were comparable.

For two-photon imaging, explanted tumors were superfused with temperature-controlled medium bubbled with 95%O_2/5%CO_2, similarly to what has been described for explanted PLNs (28, 29). GFP$^+$ cells within progressing tumors in nonvaccinated animals were generally scarce. In addition, the motility of these cells was low (Video S3, available at http://www.jem.org/cgi/content/full/jem.20060710/DC1) and did not change when imaging was performed on days 2, 3, and 4 after the vaccine boost (Fig. 2 d and Table I). In contrast, in vaccinated animals T cell motility increased markedly from day 2 (Video S4) to day 4 (Video S5) after the second vaccination (Fig. 2 d and Table I). Analysis of the migration pattern of nonconfined GFP$^+$ cells (defined by a

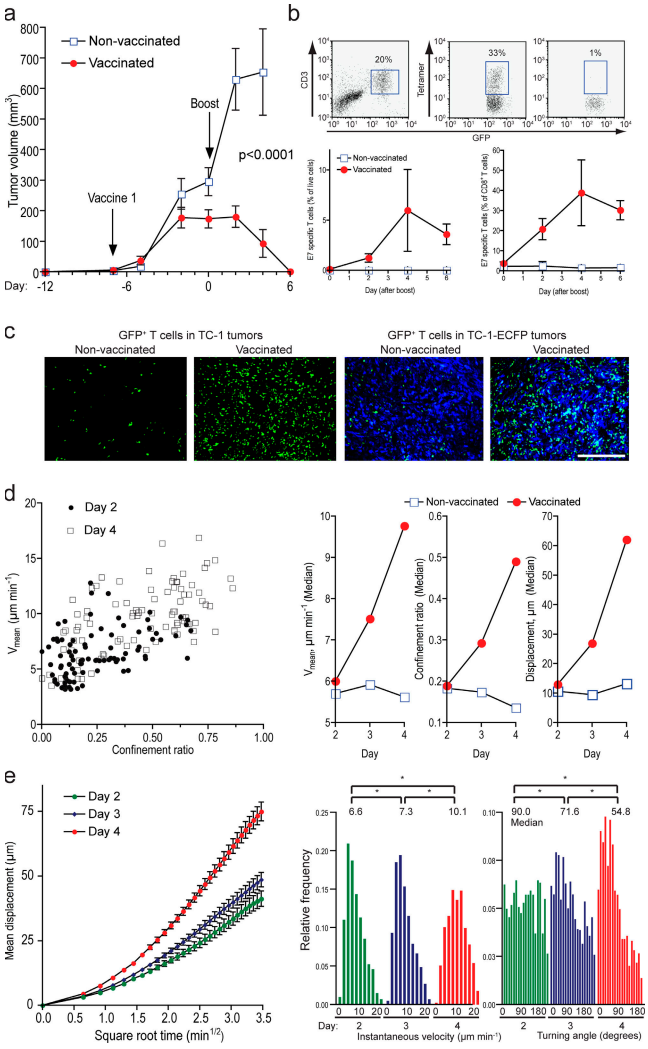

Figure 2. T cells migrate randomly within explanted tumors and become highly motile during tumor regression. (a) The tumor volume was measured in control and vaccinated animals for up to 19 d. (b) Single cell suspensions of tumors were analyzed for the presence of E7-specific CD8$^+$ T cells using MHC class I tetramers. A representative FACS profile is shown in the top panel. The percentage of E7-specific cells within total live cells or CD8$^+$ T cells was determined in a time course (bottom panels). (c) Sections of formalin-fixed TC-1 and TC1-ECFP (blue) tumors were analyzed with immunofluorescence microscopy for the presence and distribution of GFP$^+$ cells (green). Bar, 200 μm. (d) Two-photon imaging was used to track and measure migratory characteristics of GFP$^+$ T cells within explanted tumors (correlation between V_{mean} and confinement ratio: day 2: $r = 0.48$, $P < 0.0001$; day 4: $r = 0.55$, $P < 0.0001$). See Table I for statistical analysis of migratory parameters. (e) Mean displacement plots (left) and the relative frequency distribution of instantaneous velocities and turning angles (right) of nonconfined T cells in vaccinated animals are depicted (*, $P < 0.001$).

Table I. Migratory properties of GFP$^+$ T cells in TC-1 tumors

	No. of tumors	No. of regions	No. of tracks	Mean velocity[a]	Confinement ratio[a]	Displacement[a]
Sample	*n*	*n*	*n*	μm min^{-1}	no unit	μm
Nonvaccinated day 2	2	5	50	5.7 (4.1,8.1)	0.18 (0.08,0.34)	10.6 (5.3,29.8)
Nonvaccinated day 3	3	5	50	5.9 (4.4,7.8)	0.17 (0.10,0.31)	9.5 (6.5,22.5)
Nonvaccinated day 4	2	5	50	5.6 (3.8,7.7)	0.14 (0.09,0.25)	13.2 (5.2,18.6)
Vaccinated day 2	4	9	90	6.0 (4.9,7.9)	0.19 (0.11,0.37)	13.0 (6.5,34.0)
Vaccinated day 3	3	11	110	7.5 (5.6,9.3)	0.29 (0.16,0.49)	26.9 (13.3,49.1)
Vaccinated day 4	2	9	90	9.8 (7.6, 12.0)	0.49 (0.22,0.63)	62.1 (21.6,85.9)
Samples compared[b]						
Vaccinated days 2/3				$P < 0.001$	$P < 0.05$	$P < 0.01$
Vaccinated days 3/4				$P < 0.001$	$P < 0.01$	$P < 0.001$
Vaccinated days 2/4				$P < 0.001$	$P < 0.001$	$P < 0.001$
Nonvaccinated days 2/ 3				$P > 0.05$	$P > 0.05$	$P > 0.05$
Nonvaccinated days 3/4				$P > 0.05$	$P > 0.05$	$P > 0.05$
Nonvaccinated days 2/4				$P > 0.05$	$P > 0.05$	$P > 0.05$
Nonvaccinated day 2/vaccinated day 2				$P > 0.05$	$P > 0.05$	$P > 0.05$
Nonvaccinated day 2/vaccinated day 4				$P < 0.001$	$P < 0.001$	$P < 0.001$

[a]Medians of the analyzed migratory parameters are shown. The values in parenthesis indicate the interquartile range.
[b]p-values were calculated with Dunn's multiple comparison test.

mean velocity (V_{mean}) $\geq$ 5 μm min^{-1} and a confinement ratio $\geq$ 0.25) revealed a linear relationship between the square root of time and mean displacement of migrating T cells at all time points examined, consistent with random migration (Fig. 2 e, left; reference 28). However, their total displacement increased from day 2 to day 4, relating to a significant increase in instantaneous migratory velocity (Fig. 2 e, middle and left). This could be associated with changes in the local micromilieu, such as remodeling of ECM components. In addition, recognition of cognate antigen may support a highly motile phenotype of T cells (see below). We also observed a decrease in turning angles of migrating T cells over time (Fig. 2 e right), indicating a higher propensity of the cells to crawl in a more linear fashion between individual tracking segments. This phenomenon may be explained by a decrease in the number of tumors cells and hence a diminished likelihood of cellular interactions that may divert the migratory path of T cells.

Of note, our experiments exposed the highly polarized morphology of actively migrating T cells, revealing lamellipodia at the leading edge and trailing uropods (Fig. 3 and Video S6, available at http://www.jem.org/cgi/content/full/jem.20060710/DC1). In addition, as indicated by second harmonic generation signals, T cells crawled along ECM fibers (Video S6), suggesting that these structures may be used as guidance cues through the interstitial space. These results are consistent with previous reports demonstrating fiber-associated locomotion of MTLn3 mammary adenocarcinoma cells in the tumor microenvironment in vivo (39).

TILs engage in long- and short-term interactions with tumor cells

Next, we directly determined the nature of TIL contacts with TC-1 cells stably expressing enhanced cyan fluorescent

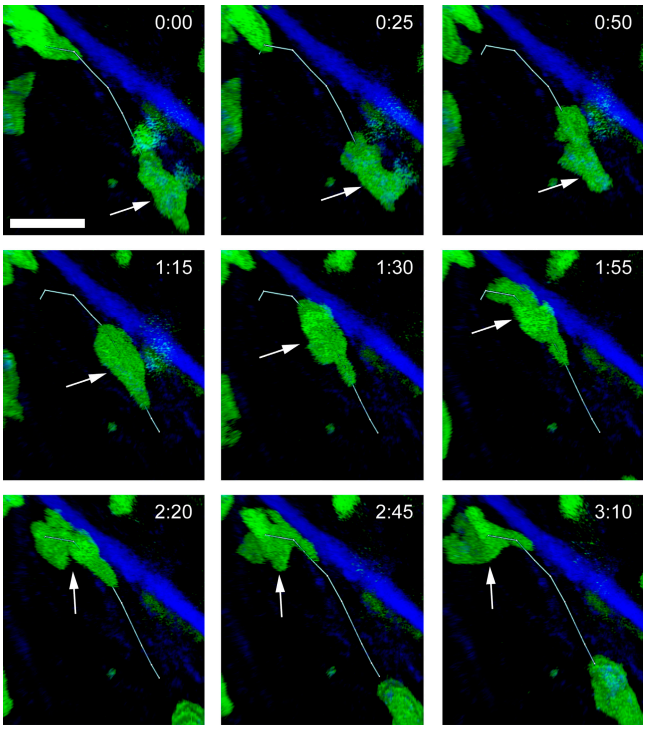

Figure 3. Migrating TILs reveal a polarized morphology and crawl along fibers of the ECM. A TC-1 tumor was explanted on day 4 after the vaccine boost, and T cells (green) and ECM fibers (blue; second harmonic generation signals) were visualized by two-photon microscopy. Imaging was performed as described in Materials and methods, except that x-y planes were 67.5 by 67.5 μm with 0.13 μm pixel^{-1}. Note the formation of lamellipodia at the leading edge and the uropod at the trailing end of the cells. One individual cell is followed over time (indicated by arrow and track). Numbers indicate minutes/seconds. Bar, 12 μm.

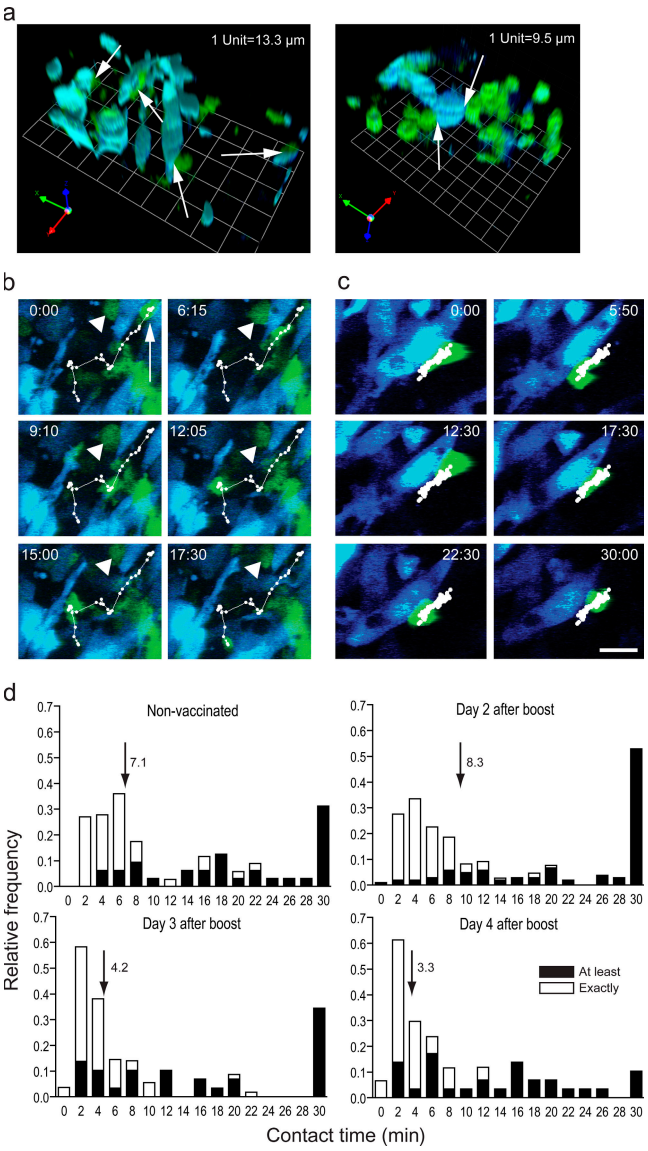

Figure 4. TILs engage in short- and long-term interactions with tumor cells in explanted tumors. GFP$^+$ T cells (green) and TC-1-ECFP tumor cells (blue) were imaged simultaneously with two-photon microscopy. (a) Three-dimensional reconstruction of areas containing T cell–tumor cell contacts (arrows) 2 (left) and 3 (right) d after the vaccine boost. (b) A T cell undergoing a stable interaction (arrowhead) with a tumor cell and a T cell interacting sequentially (arrow, track) with several tumor cells are shown. (c) A T cell crawling along the surface of a tumor cell is depicted (track). Numbers in a and b indicate minutes/seconds. Bar, 13 µm. (d) The contact times of T cells interacting with tumor cells are charted. Open bars, conjugates that were tracked for the entire observation period; filled bars, conjugates that were present either at the beginning or at the end of the observation period (nonvaccinated: $n = 69$ interactions; day 2 after boost: $n = 221$ interactions; day 3 after boost: $n = 83$ interactions; day 4 after boost: $n = 90$ interactions). Arrows and numbers depict the median interaction times.

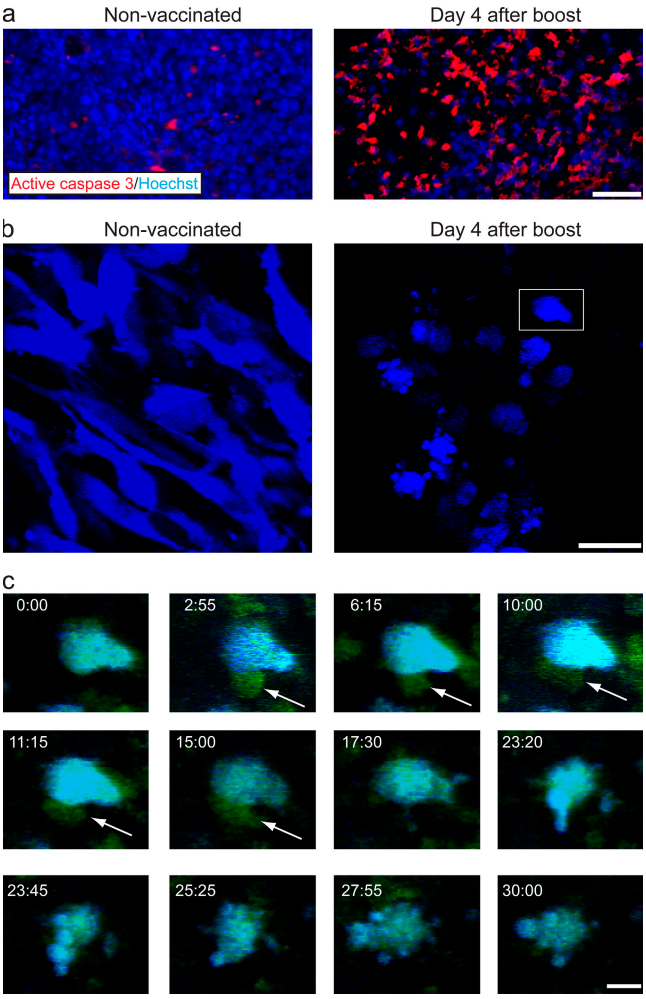

Figure 5. Contact with T cells precedes initiation of apoptosis in tumor cells. (a) On day 4 after vaccination, tissue sections were stained with an antibody against active caspase 3 (red) and cell nuclei were stained with Hoechst 33258 (blue). Bar, 100 µm. (b) Explanted TC-1 ECFP tumors were imaged with two-photon microscopy. Bar, 26 µm. (c) The boxed tumor cell in b was followed in detail for 30 min. The tumor cell was contacted by a T cell (green, arrow) before it disintegrated. Numbers indicate minutes/seconds. Bar, 9 µm.

protein (ECFP). Fig. 4 a shows three-dimensional reconstructions of representative areas in tumors 2 and 3 d after the vaccine boost. The arrows in Fig. 4 a depict direct GFP$^+$ T cell and ECFP$^+$ tumor cell interactions. Dynamic analysis of these interactions revealed two principal interaction patterns between GFP$^+$ and ECFP$^+$ cells 2 d after the vaccine boost. Approximately 50% of interacting T cells engaged in firm, long-term contacts with ECFP$^+$ cells that lasted for the entire observation period (≥30 min; Video S7, available at http://www.jem.org/cgi/content/full/jem.20060710/DC1, and Fig. 4, b–d). Although some of these cells remained stably in the same position (Fig. 4 b), others crawled slowly along the tumor surface without detaching (Video S8 and Fig. 4 c). The other half of interacting TILs established sequential short-term interactions with tumor cells (Video S7 and Fig. 4, b and d). 3 and 4 d after the vaccine boost we observed a decrease in the number of long-lasting contacts between

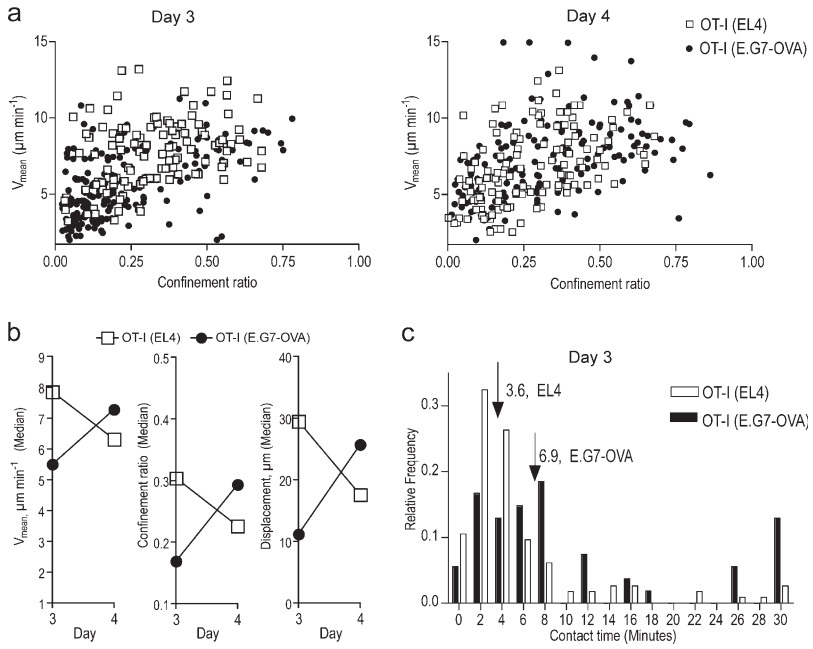

Figure 6. Tumor antigen–specific T cells engage in direct contact with tumor cells and maintain high motility in the presence of cognate antigen. (a) DPE^{GFP}xOT-I CTLs were tracked in explanted EL4 and EG.7-OVA tumors using two-photon microscopy, and their migratory parameters were measured (correlation between V_{mean} and confinement ratio: EL4, day 3: $r = 0.38$, $P < 0.0001$; EG.7-OVA, day 3: $r = 0.52$, $P < 0.0001$; EL4, day 4: $r = 0.55$, $P < 0.0001$; E.G7-OVA, day 4: $r = 0.54$, $P < 0.0001$). (b) Shown are the dynamic changes in migratory parameters between days 3 and 4 after adoptive transfer. See Table II for statistical analysis. (c) The duration of interactions between DPE^{GFP}xOT-I CTL and E.G7-OVA-ECFP or EL4-ECFP tumor cells was measured. The relative frequencies of contact times are charted (EL4: $n = 114$ interactions; E.G7-OVA: $n = 54$ interactions; $P = 0.0005$ determined by Mann-Whitney test). Arrows and numbers depict the median interaction times.

T cells and tumor cells (Fig. 4 d; days 2/3, $P < 0.001$; days 2/4, $P < 0.001$). We also determined the quality of TIL interactions within progressing tumors. As mentioned above, we usually detected only a few GFP$^+$ cells within tumor areas necessitating the acquisition of multiple fields of view per tumor. Of those GFP$^+$ cells that interacted with tumor cells, approximately two thirds engaged in short-term interactions (~5 min), whereas one third of the conjugates remained for 30 min or longer (Fig. 4 d). This suggests that even in unvaccinated animals, tumor antigen–specific T cells may develop, but other mechanisms may prevent their expansion/activity resulting in progressive tumor growth (1, 7, 8).

Tumor cell disintegration follows T cell contacts

A likely consequence of T cell attack on tumors is the induction of tumor cell apoptosis, which may be mediated by direct cytotoxicity or indirect effects on the tumor stroma. Indeed, 4 d after the vaccine boost most tumor cells were undergoing apoptotic cell death as defined by immunostaining for active caspase 3 (Fig. 5 a). By two-photon microscopy we show that

Table II. Migratory properties of OT-I cells in EL4 and E.G7-OVA tumors

	No. of tumors	No. of regions	No. of tracks	Mean velocity[a]	Confinement ratio[a]	Displacement[a]
Sample	*n*	*n*	*n*	μm min^{-1}	no unit	μm
EL4 (day 3)	4	16	110	7.9 (6.0,9.2)	0.30 (0.19,0.44)	29.5 (14.2,46.2)
E.G7-OVA (day 3)	4	16	180	5.5 (4.0,7.5)	0.17 (0.09,0.33)	11.2 (4.9,29.0)
EL4 (day 4)	5	19	130	6.3 (4.7,8.6)	0.23 (0.12,0,39)	17.6 (6.7,38.1)
E.G7-OVA (day 4)	5	18	160	7.3 (5.4,8.7)	0.29 (0.16,0.48)	25.7 (10.6,51.4)
Samples compared[b]						
EL4 (day 3)/EL4 (day 4)				$P < 0.01$	$P > 0.05$	$P < 0.05$
E.G7-OVA (day 3)/E.G7-OVA (day 4)				$P < 0.001$	$P < 0.001$	$P < 0.001$
EL4 (day 3)/E.G7-OVA (day 3)				$P < 0.001$	$P < 0.001$	$P < 0.001$
EL4 (day 4)/E.G7-OVA (day 4)				$P > 0.05$	$P > 0.05$	$P > 0.05$

[a]Medians of the analyzed migratory parameters are shown. The values in parenthesis indicate the interquartile range.
[b]p-values were calculated with Dunn's multiple comparison test.

under control conditions TC-1 cells revealed an elongated spindle-shaped morphology. In contrast, in regressing tumors, TC-1 cells frequently had a rounded shape and a condensed cell body, and were shedding blebs (Fig. 5 b), phenomena ascribed typically to apoptotic cells in cell culture. Furthermore, we directly observed the dynamics of tumor cell apoptosis in situ. Over the course of 10–20 min, apparently intact tumor cells disintegrated revealing the morphologic hallmarks of apoptosis (Fig. 5 c and Video S9, available at http://www.jem.org/cgi/content/full/jem.20060710/DC1). In some cases, T cell contacts preceded tumor cell apoptosis (Fig. 5 c and Video S9).

Recognition of cognate antigen is a critical parameter for T cell migration and cellular interactions within tumors

To better understand the molecular mechanisms mediating T cell–tumor cell interactions, we adoptively transferred in vitro–generated, OVA-specific OT-I $CD8^+$ effector CTLs into animals carrying either EL4 or E.G7-OVA tumors (Fig. S2, available at http://www.jem.org/cgi/content/full/jem.20060710/DC1). Under both circumstances, OT-I cells continued to divide in vivo for several days in all organs analyzed, including the spleen and tumors (Fig. S2 b and not depicted). We also found comparable, time-dependent accumulation of OT-I effector cells in EL4 and E.G7-OVA tumors (Fig. S2 c). Nevertheless, OT-I cells induced tumor regression and apoptosis only in E.G7-OVA tumors, which was paralleled by an increase in cell size and expression of the activation marker CD69 by OT-I cells isolated from E.G7-OVA tumors (Fig. S2, d–g).

By two-photon microscopy, we observed that 3 d after adoptive transfer a high fraction of DPE^{GFP}xOT-I T cells within E.G7-OVA, but not EL4, tumors was confined in migration (Fig. 6 a). Similar to our results in the TC-1 system, V_{mean}, confinement ratio, as well as displacement of the whole cell population within the E.G7-OVA tumors increased over time (Fig. 6, a and b, and Table II). Moreover, the nonconfined DPE^{GFP}xOT-I cells in E.G7-OVA tumors gained in migratory velocity and displacement over time, whereas their turning angles decreased (Fig. S3, available at http://www.jem.org/cgi/content/full/jem.20060710/DC1). In addition, DPE^{GFP}xOT-I cells engaged in long-term interactions with ECFP-labeled tumor cells only in the presence of cognate antigen (Videos S10 and S11, and Fig. 6 c). However, it was also evident that DPE^{GFP}xOT-I cells underwent short-term interactions with EL4 cells, indicating a default target cell–screening program of effector CTLs within target tissues (Video S12 and Fig. 6 c).

The substantial fraction of OT-I cells that was confined in migration in EL4 tumors at day 4 after adoptive transfer (Fig. 6 a) indicates that cognate signals may be necessary to maintain highly active motility of effector T cells within target tissues. Alternatively, changes in the local microenvironment, such as destruction of tumor cells, reorganization of ECM fibers, or changes in the extracellular fluid, may create more permissive conditions for T cell motility. To distinguish between these possibilities, we transferred $CD8^+$ effector CTLs generated from DPE^{GFP}xP14 cells together with unlabeled OT-I effector cells into EL4 or E.G7-OVA tumor–bearing mice. $CD8^+$ P14 T cells recognize lymphocytic choriomeningitis virus glycoprotein 33-41 and therefore lack specificity for antigens within the tumors. DPE^{GFP}xP14 cells homed to a similar extent to EL4 and E.G7-OVA tumors, and induction of tumor regression was comparable under these conditions as observed with OT-I T cell transfer alone (not depicted). Using two-photon microscopy 3 d after adoptive transfer, we found that the migratory behavior of DPE^{GFP}xP14 cells was consistent with our previous observations with DPE^{GFP}xOT-I cells (Fig. 7 a and Table S1, available at http://www.jem.org/cgi/content/full/jem.20060710/DC1). In contrast, although the latter cells revealed increased migratory motility in E.G7-OVA tumors at day 4 (Fig. 6, a–c, and Table II), DPE^{GFP}xP14 cells showed decreased migration in these tumors similarly to their behavior in EL4 tumors (Fig. 7 a and Table S1).

Because it may be argued that P14 and OT-I cells sequester to different microcompartments within tumors, and, hence, show different migratory behavior, we also cotransferred differentially labeled cells into the same tumor-bearing animals. To this end, antigen-primed P14 and OT-I T cells were transduced with retroviruses encoding for enhanced yellow fluorescent protein (EYFP) and ECFP, respectively.

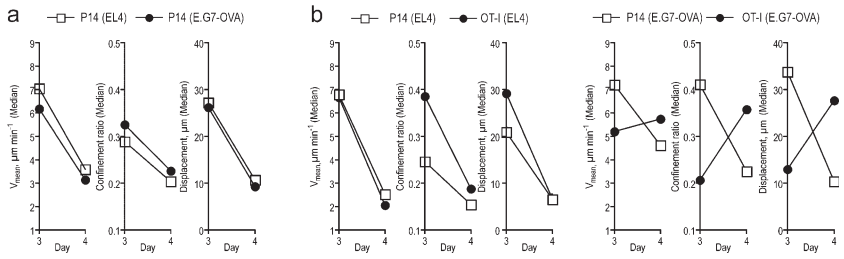

Figure 7. Recognition of cognate antigen is necessary to sustain motility of TILs. (a) Effector CTLs generated from DPE^{GFP}xP14 mice were transferred together with unlabeled OT-I effector CTLs into EL4 or E.G7-OVA tumor-bearing animals. Imaging was performed 3 and 4 d later, and migratory characteristics were determined. See Table S1 for statistical analysis. (b) P14-EYFP and OT-I-ECFP CTL were cotransferred into mice carrying EL4 or E.G7-OVA tumors. 3 and 4 d later, cells were simultaneously visualized in the same fields of view and migratory characteristics were determined. See Tables S2 and S3 for statistical analysis.

Transduced OT-I cells induced E.G7-OVA tumor regression similarly to untransduced OT-I cells (not depicted). Two-photon-microscopy revealed that OT-I-ECFP and P14-EYFP cells homed to the same microcompartments within the tumors (Videos S13 and S14, available at http://www.jem.org/cgi/content/full/jem.20060710/DC1). Fig. 7 b depicts the migratory characteristics of the cells visualized in the same fields of view 3 and 4 d after adoptive transfer. Consistent with the results obtained with DPE^{GFP}xP14 cells (Fig. 7 a), we found that P14-EYFP cells decreased their migration between days 3 and 4 regardless of the presence or absence of cognate antigen (Fig. 7 b and Tables S2 and S3). In contrast, although OT-I-ECFP cells were less active in EL4 tumors over time, a clear increase in their migratory behavior was observed in E.G7-OVA tumors between days 3 and 4 after adoptive transfer (Fig. 7 b, Tables S2 and S3, and Videos S13 and S14). Because, under these conditions, P14 and OT-I cells were exposed to the same microenvironmental cues, these results support the conclusion that the recognition of cognate antigen by TILs at the effector site is important for the maintenance of a highly active migratory phenotype.

TILs interact physically with macrophages within tumors

Of note, we found that a considerable proportion of confined DPE^{GFP}xOT-I cells within E.G7-OVA tumors did not contact ECFP-expressing tumor cells, but rather interacted with cells containing autofluorescent particulate material. Using immunofluorescence microscopy of tissue sections, we show that these cells represent F4/80^{+} macrophages (Fig. 8 a). We frequently observed that migrating CTLs in E.G7-OVA tumors arrested upon encounter with such macrophages, and long-lasting interactions resulted (Fig. 8 b and Video S15, available at http://www.jem.org/cgi/content/full/jem.20060710/DC1). These data are consistent with the hypothesis that antigen-presenting cells in the tumor microenvironment cross-present tumor-associated antigens (16), and that T cells interact with macrophages in an antigen-specific manner (40).

Migratory behavior of TILs within tumors in vivo

Although a major advantage of our tumor explant model is that the imaging conditions can be kept constant between individual experiments, it should be noted that the lack of blood supply, lymphatic drainage, and innervation may have influenced the behavior of T cells within tumors. To gain further insight into this issue, we analyzed DPE^{GFP}xOT-I T cell migration within subcutaneously implanted EL4 tumors in vivo. When areas deep within the tumor were imaged (which represents the areas typically visualized in our explant model), T cells revealed a polarized morphology reminiscent of the cells in the explant model (Video S16, available at http://www.jem.org/cgi/content/full/jem.20060710/DC1). No difference was found in migratory velocities and confinement ratios of DPE^{GFP}xOT-I cells under the two conditions (Fig. 9 a). Moreover, displacement plots revealed that at the population level, TILs migrated randomly (Fig. 9 b). Collectively, these results show that our explant model faithfully recapitulates the migratory behavior of T cells in the tumor microenvironment in vivo.

DISCUSSION

The success of immunotherapeutic strategies against cancer depends on the generation of effective tumor antigen–specific T cells that must not only enter the tumor tissue, but must also be able to traverse the interstitial space and finally interact with target cells. A prerequisite for the optimization of such strategies is the dissection of the cellular and molecular processes that ultimately lead to tumor cell destruction.

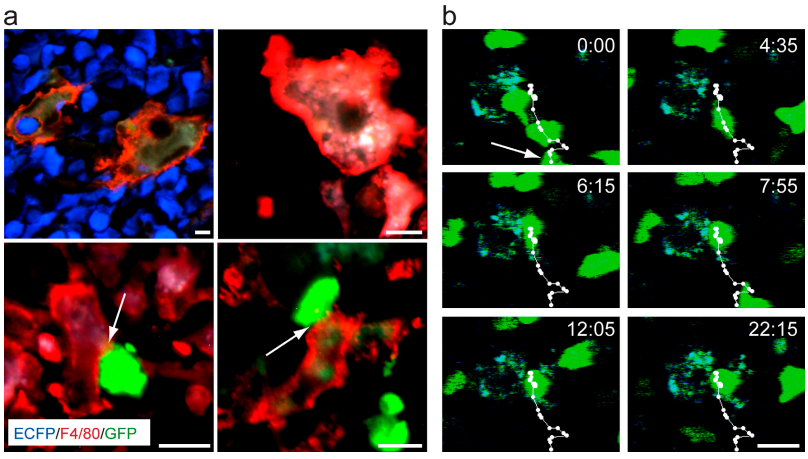

Figure 8. Tumor antigen–specific T cells engage in physical contact with macrophages in explanted tumors. (a) E.G7-OVA-ECFP tumors were analyzed by immunofluorescence microscopy 4 d after adoptive transfer of DPE^{GFP}xOT-I CTL. F4/80^{+} cells (red) contained autofluorescent particulate material. Contacts between T cells (green) and F4/80^{+} cells are depicted by arrows. Bars, 10 μm. (b) Two-photon imaging shows a crawling T cell (green) that arrests after contacting a macrophage (cyan) within explanted E.G7-OVA-ECFP tumors. The arresting T cell is highlighted with an arrow and a track. Numbers indicate minutes/seconds. Bar, 13 μm.

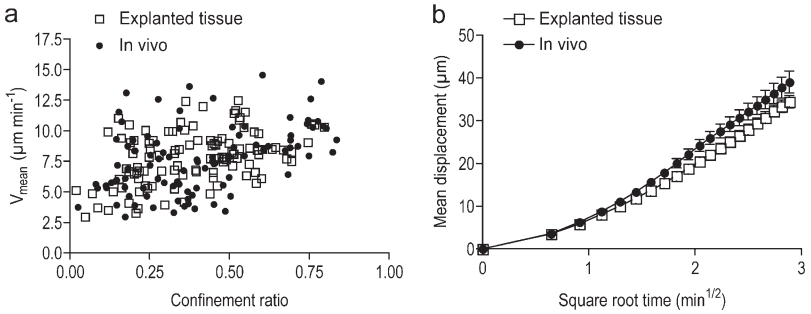

Figure 9. Migratory characteristics of OT-I effector CTLs within EL4 tumors in vivo. EL4 cells were injected subcutaneously into the flanks of C57BL/6 mice. DPE^{GFP}xOT-I effector CTLs were adoptively transferred 8 or 9 d later. After an additional 3 d, two-photon imaging was performed in surgically exposed tumors ($n = 4$) of anesthetized mice. (a) Migratory parameters were determined (circles) and are shown in comparison to data obtained in tumor explants (quadrangles). For both conditions, 21 consecutive video frames were analyzed (V_{mean} [median]: in vivo: 7.7 μm min^{-1}, explants: 8.1 μm min^{-1}; $P = 0.33$; confinement ratio [median]: in vivo: 0.37, explants: 0.39; $P = 0.91$). (b) The mean displacement of nonconfined cells ($V_{mean} \geq 5$ μm min^{-1}, confinement ratio ≥ 0.5) within explanted tumor tissue or in vivo was calculated and charted over time.

Our study provides a new vista of the dynamics and orchestration of T cell behavior within tumors, which is an essential step toward understanding the complex cellular interplay at such sites.

In this study, we made use of a tumor explant model for two-photon imaging of TIL behavior. This model guarantees highly reproducible experimental conditions and facilitates imaging over prolonged periods of time without significant movement of the tissue, thereby reducing motion artifacts. Dynamic immune cell imaging in intact explanted tissues, including PLNs, thymic lobes, and the spinal cord, has now been widely used to study the migratory and interactive behavior of lymphocytes and dendritic cells (27, 28, 41). However, a caveat with explanted tissue models is the lack of nutrient supply that may alter the performance of cells as compared with their counterparts in tissues in vivo. Nevertheless, in the case of PLNs, careful comparisons of tissues in situ and in explants have revealed very similar T cell behavior (22, 28–30). Moreover, experiments performed in our study demonstrate that OT-I CTLs in EL4 tumor explants do not behave differently than in tumors in vivo, which confirms the validity of our approach. This notwithstanding, future studies will aim to dissect TIL–target cell interactions within tumors in vivo and the relationship between TILs, tumor cells, the blood and lymphatic vasculature, as well as the nervous system and other cellular components of this particular environment.

We showed that at the population level, TILs migrated randomly within the tumor microenvironment both in the tumor explants and within tumors in situ. This finding was unexpected, as it argues against the concept of TIL guidance by long-range chemokine gradients in the interstitial space (14, 15). Random migration of TILs is in contrast to the behavior of tumor cells that follow more directed migratory routes in vivo as an integral part of the metastatic process via blood/lymphatic vessel invasion (39). Thus, there appear to be fundamental mechanistic differences in the movement of individual cellular components within the tumor microenvironment, implying the involvement of distinct regulatory mechanisms. In vitro studies have shown that T cells can use collagen fibers as a scaffold for their migration (42). Thus, an attractive hypothesis would be that the ECM provides migratory cues for TILs. Consistent with this hypothesis, we found intimate contacts between TIL and ECM fibers (Fig. 3 and Video S6). Integrins and other adhesion molecules, such as CD44, may be involved in this contact-dependent migration of TILs. Examination of T cells deficient in certain adhesion receptors will help gain further insight into these open questions.

From a functional viewpoint, similarly to what has been proposed for naive T cells in PLNs, random migration of effector T cells within target organs may maximize the likelihood for target cell contacts (28, 30). Thus, it appears that effector T cells in the periphery very actively screen their microenvironment for the presence of cognate antigen. Interestingly, in contrast to naive T cells within LNs, effector CTLs required the presence of cognate antigen within the target site to maintain an active migratory program (Figs. 6 and 7). This was indicated by the observation that effector CTLs that reached the target organ in the absence of cognate antigen reduced migratory velocities and displacement between 24 and 48 h after tissue entry. These observations were consistent for TILs in progressing and regressing tumors, indicating that changes in the microenvironment induced by an efficient antitumor T cell response per se are not sufficient to support high migratory motility of effector CTLs. Nevertheless, it is conceivable that, after antigen contact, reduced tumor cell densities and/or remodeling of the ECM in regressing tumors contributes to the detectable increase in T cell motility. Furthermore, it should be noted that although the viability of OT-I cells in EL4 and E.G7-OVA tumors 4 d after adoptive transfer was similar, we cannot exclude the possibility that in the absence of cognate antigen, effector T cells undergo programmed cell death at earlier time points as compared with T cells that encounter antigen within tumors. Collectively, we propose that recognition of cognate antigen

within tumors is a prerequisite for efficient migration of TILs. This notion bears consideration for adoptive T cell transfer approaches, as it may suggest that in the absence of cognate antigen, CTLs rapidly lose their high speed target–searching capability.

T cell infiltration into tumors in nonvaccinated animals was sparse. Those T cells that successfully entered this microenvironment were largely inactive in their migration, and their migratory behavior did not change over the course of 3 d. This indicates that the cells either did not reencounter cognate antigen in the tumors (which may be necessary for their reactivation directly within the effector site; see also Fig. 6) and/or the presence of factors that inhibit the active migration of T cells. However, it is interesting to note that some TILs even in progressing tumors were found to stably interact with tumor cells, which may favor the hypothesis of migratory suppression under these conditions.

The precise identity of the cells targeted by TILs, as well as the exact mechanisms by which T cells induce tumor regression, has been matter of long-standing debate. It has been suggested that MHC-restricted recognition of antigens on tumor cells within the tumor microenvironment is crucial for T cell–mediated tumor rejection (7). However, an emerging concept postulates the importance of antigen cross-presentation by stromal cells for the induction of tumor regression (16). Our study reconciles these claims by demonstrating that TILs physically contact both tumor cells and tissue macrophages.

The fact that approximately half of the observed cognate antigen–dependent interactions of TILs with tumor cells were long-lasting would be consistent with direct cytotoxicity by TILs via the secretion of proapoptotic factors, including granzymes and perforin. Moreover, the protracted nature of these interactions may indicate the formation of immunologic synapses (43), which have also been demonstrated to develop, for instance, between effector CTLs and virus-infected target cells in vivo (44). It will be interesting to compare the dynamics of formation as well as the molecular composition of immunologic synapses between naive T cells and antigen-presenting cells during the priming phase, and effector CTLs and target cells during the efferent phase of the immune response. This will give important insights into the mechanisms of target cell destruction by TILs.

The other half of TIL–tumor cell interactions was short-lived, and TILs often engaged with multiple consecutive tumor cells within short periods of time. Similar cellular encounters that occur between T cells and dendritic cells in collagen matrices in vitro are sufficient to induce activation of T cells (45). Thus, it is conceivable that effector T cells also integrate signals from such consecutive interactions with tumor cells necessary for maintaining their activated state and/or the induction of cytokine production (for example, IFN-γ).

Recognition of cross-presented antigen on macrophages by TILs could result in TIL activation followed by cytokine production (for instance, IFN-γ). Reciprocally, the secretion of IFN-γ may lead to the activation of macrophages and induce the production of tumoricidal mediators, including reactive oxygen species or nitric oxide (46). Interestingly, IFN-γ may be released directly into the immunologic synapse, which could establish a high local concentration of the cytokine and preferential activation of the adjacent macrophage (47). Of note, stromal cells may themselves be targets for cytotoxic attack by TILs. Indeed, a recent study has shown that destruction of $CD11b^+$ stromal cells that cross-present tumor antigen can contribute to the elimination of established tumors in which tumor cells had lost the capability to express target antigen (antigen loss variants; reference 17).

In conclusion, our results provide evidence that direct interactions of TILs with antigen-presenting cells and tumor cells are integral elements of the effector phase of the antitumor immune response. Our model provides the basis for further elucidation of the molecular machinery involved in the migration of TILs as well as their interactions with target cells within tumors.

MATERIALS AND METHODS

Mice. We used a transgenic mouse strain (DPE^{GFP}; crossed to the C57BL/6 background for 10 generations) in which GFP is expressed by all T cells. OT-I mice (The Jackson Laboratory) and P14 mice (provided by E.J. Wherry, The Wistar Institute, Philadelphia, PA) were crossed with DPE^{GFP} mice (DPE^{GFP}xOT-I, DPE^{GFP}xP14). C57BL/6 wild-type mice were obtained from Charles River Laboratories. Experimental protocols were approved by the Institutional Animal Care and Use Committee of The Wistar Institute.

Reagents. CD3, IgG, L-selectin, CD44, CD69, and CD8 antibodies (BD Biosciences); an anti-active caspase 3 rabbit serum (R&D Systems); Alexa 546–conjugated goat anti–rabbit IgG; CFSE (Invitrogen); and bisbenzimide (Hoechst 33258; Sigma-Aldrich) were used. An E7-specific MHC class I tetramer was provided by S. Albelda (University of Pennsylvania, Philadelphia, PA). SIINFEKL peptide was purchased from Alpha Diagnostic International.

Tumor experiments. EL4 and E.G7-OVA thymoma cells were purchased from the American Type Culture Collection. TC-1 was obtained from T.C. Wu (Johns Hopkins University, Baltimore, MD). TC-1-ECFP cells were generated by transfection with a pcDNA3.1/ECFP construct. EL4-ECFP and E.G7-OVA-ECFP lines were generated using a retroviral plasmid containing ECFP (provided by L. Beverly and A. Capobianco, The Wistar Institute). Individual ECFP-expressing clones were selected that had similar in vitro and in vivo growth characteristics as the parental cell line (not depicted and Fig. S4).

For all experiments, 10^6 tumor cells were injected subcutaneously in the flank of mice. TC-1 tumor-carrying mice were injected intramuscularly with adenovirus human strain 5–expressing E7 protein (2×10^7 pfu) in 100 μl PBS or with PBS alone 5 and 12 d after tumor cell inoculation. EL4 or E.G7-OVA tumor-carrying mice were injected intravenously with 2×10^7 DPE^{GFP}xOT-I effector CTLs 8 d after tumor injection. In some experiments, OT-I effector CTLs were mixed with DPE^{GFP}xP14 (2×10^7 each). Effector CTLs were generated as described previously (48). In brief, splenocytes from TCR transgenic mice were stimulated with the respective cognate peptides (1 μg/ml) for 1 h, washed, and incubated for 2 d. Thereafter, cells were cultured in the presence of 20 ng/ml IL-2 for an additional 5–6 d. Medium was changed every other day.

For covisualization experiments, P14 and OT-I cells were stimulated with peptides as described above. 24 h later, the cells were transduced with MIGR1-based retroviral plasmids containing either the ECFP or EYFP coding sequence (provided by S. Reiner, University of Pennsylvania) using

previously published protocols (49). In brief, 3–5 × 10^6 cells were resuspended in 1 ml of viral supernatant containing 8 μg/ml polybrene and centrifuged at 6,000 *g* for 90 min at 25°C. Thereafter, the cells were cultured in the presence of 20 ng/ml IL-2. Media was changed daily until use.

Flow cytometry. Excised tumors were cut into small pieces and incubated in HBSS containing 10 mg ml^{-1} collagenase D (Roche) and 1 mg ml^{-1} DNase I (Roche). Single cell suspensions were stained and analyzed using a FACSCalibur flow cytometer (Becton Dickinson). Data were analyzed with FlowJo software (Tree Star).

Immunofluorescence staining. PLNs and tumor tissue were either fixed overnight in 4% formaldehyde/10% sucrose at 4°C (for analysis of GFP^+ cells) or directly snap-frozen in liquid nitrogen. Immunostaining was performed as described previously (50).

Tissue preparation for live cell imaging. For the tissue explant model, mice were killed by CO_2 asphyxiation and the desired tissues were removed. Subcutaneously implanted tumors were usually well demarcated and could be separated easily from surrounding fat and connective tissue, thus inducing only minimal mechanical stress. Immediately after preparation, tissues were transferred into an imaging chamber (Warner Instruments) and stabilized either with superglue (LNs) or with a mesh (tumors). Tissues were continuously superfused with RPMI medium containing 10% fetal bovine serum and bubbled with 95% oxygen and 5% carbon dioxide as described previously (28, 29). The temperature was maintained at 36.5°C.

For in vivo imaging of tumors, we adapted a previously established model of subiliac LN preparation/imaging (51). In brief, tumors were implanted into the flanks of C57BL/6 mice, and DPE^{GFP}xOT-I effector cells were transferred 8 or 9 d later. After an additional 3 d, mice were anesthetized and a skin flap with the embedded tumor was prepared by separating the skin from the underlying abdominal wall. This procedure exposed the surface of the tumors without the need for further dissection of connective tissue or fat cells, thus avoiding damage to feeding and draining blood vessels. The preparation was then immersed in prewarmed physiologic saline solution (36.5°C). The temperature was controlled and adjusted as needed.

Two-photon microscopy and image analysis. Two-photon imaging was performed on a Prairie Technology Ultima System attached to an Olympus BX-51 fixed-stage microscope equipped with 20× (NA 0.95) and 40× (NA 0.8) water immersion objectives. The setup included external nondescanned dual-channel reflection/fluorescence detectors and a diode-pumped, wideband mode–locked Ti:Sapphire femtosecond laser (720–950 nm, <140 fs; 90 MHz; Coherent Chameleon).

The samples were exposed to polarized laser light at a wavelength of 920 (T cell migration studies) or 890 nm (T cell–target cell interaction studies). Emitted light was separated with a filter set (dichroic mirror, 495 nm; bandpass, 520/35 nm; bandpass, 460/50 nm). In experiments where ECFP- and EYFP-expressing cells were covisualized, an alternative filter set was used (dichroic mirror, 515 nm; bandpass, 485/15 nm; bandpass, 522.5/12.5 nm). z-stacks of a series of x-y planes of 284 by 284 μm at a resolution of 0.55 μm $pixel^{-1}$ (migration studies) or of 142 by 142 μm at a resolution of 0.28 μm $pixel^{-1}$ (interaction studies) with a total thickness of 30 μm (step size, 6 μm) were captured every 25 s using Prairie View acquisition software (Prairie Technologies). Typically, the tumor samples were imaged at a depth of 50–150 μm below the surface.

Three-dimensional image stacks were transformed into movies using Volocity software (Improvision). Mean migration velocities, cellular displacement, and confinement ratios (total length of track divided by distance between starting and end point) were calculated for 12'55" (tumors) or 7'5" (LNs) as described previously (25). Instantaneous velocity was defined as the velocity of a cell during a 50" observation period (25). The turning angle was defined as the deviation of one segment of a track from the preceding one (25). Measurements were typically performed on 31 consecutive frames of the videos, with the exception of the in vivo tumor experiments, where 21 frames were evaluated. For the measurement of T cell–target cell interactions, T cells in a field of view were randomly selected at the start of the acquisition period and followed until they either left the field of view or until the end of the imaging sequence. Cellular contacts were defined as the absence of a space (empty pixels) between fluorescent T cells and tumor cells or macrophages in the same x-y plane. Imaging for these experiments was conducted for 30 min.

Statistical analysis. For group comparisons of normally distributed samples (KS test), one-way ANOVA followed by the Bonferroni test was used. Otherwise, groups were compared using the Kruskal-Wallis followed by Dunn's multiple comparison test. For comparisons of two samples, the Student's *t* test (normally distributed) or the Mann-Whitney test (not normally distributed) was used. A difference was considered significant if $P < 0.05$. The error bars in all charts represent standard errors of the mean. To test if values for the mean velocity correlated to the confinement ratio, Spearman's rank correlation coefficient was calculated.

Online supplemental material. Fig. S1 demonstrates that a high fraction of TILs both in vaccinated and nonvaccinated tumors is activated. Fig. S2 characterizes the growth behavior of EL4 and E.G7-OVA tumors as well as TIL phenotype and function after adoptive transfer. Fig. S3 shows the migratory properties of adoptively transferred nonconfined TILs in EL4 and E.G7-OVA tumors. Fig. S4 analyzes the growth behavior of TC-1 ECFP tumors in vaccinated and nonvaccinated mice, and characterizes the migratory properties of TILs. Table S1 shows the motility characteristics of P14 cells within EL4 and E.G7-OVA tumors. Table S2 depicts the motility of simultaneously imaged P14-EYFP and OT-I-ECFP cells in EL4 tumors. Table S3 provides the motility of P14-EYFP and OT-I-ECFP cells in E.G7-OVA tumors. Videos S1 and S2 show endogenous naive T cells migrating within a PLN. Videos S3–S5 show migration of endogenous TILs in TC-1 tumors. Video S6 shows a high resolution sequence of a TIL crawling along an ECM fiber. Videos S7 and S8 show TILs in vaccinated mice that interact with tumor cells. Video S9 shows a tumor cell in a vaccinated mouse that disintegrates after being targeted by TILs. Videos S10–S12 show adoptively transferred OT-I cells interacting with E.G7-OVA or EL4 tumor cells. Videos S13 and S14 show P14-EYFP and OT-I-ECFP TIL simultaneously imaged within E.G7-OVA tumors. Video S15 shows adoptively transferred OT-I cells interacting with a macrophage. Video S16 shows migrating TILs within an EL4 tumor in vivo. The online supplemental material is available at http://www.jem.org/cgi/content/full/jem.20060710/DC1.

We thank Dr. Steven Albelda (University of Pennsylvania) for providing the E7-tetramer, Dr. Anthony Capobianco and Mr. Levi Beverly (The Wistar Institute) for providing a retroviral plasmid containing ECFP, Drs. Steven Reiner and Ichiko Kinjyo (University of Pennsylvania) for providing retroviral plasmids containing ECFP or EYFP, Dr. T.C. Wu (Johns Hopkins University, Baltimore, MD) for providing TC-1 cells, Dr. John Wherry (The Wistar Institute) for providing P14 mice, and Ms. Min Wang and Ms. Norma Black for technical assistance. We thank Drs. Ellen Pure, Jan Erikson, Christopher Hunter, and Steven Albelda, as well as Ms. Kim Jordan for helpful discussion.

W. Weninger was supported by a grant from the W.W. Smith Charitable Trust, a Career Development Award from the Skin Cancer SPORE, and R21 CA114114 and S10 RR021100 from the National Institutes of Health (NIH). P. Mrass is a fellow of the Max Kade Foundation, Inc., and the recipient of a Cancer Research Institute postdoctoral fellowship. This work was supported, in part, by NIH grant AI061663 to U.H. von Andrian.

P.G. Haydon has equity interest in the company Prairie Technologies, Corp., which builds and markets the two-photon microscope used in this project. The other authors declare no conflicting financial interests.

Submitted: 31 March 2006
Accepted: 26 October 2006

REFERENCES

1. Dunn, G.P., L.J. Old, and R.D. Schreiber. 2004. The three Es of cancer immunoediting. *Annu. Rev. Immunol.* 22:329–360.

2. Jager, E., D. Jager, and A. Knuth. 2003. Antigen-specific immunotherapy and cancer vaccines. *Int. J. Cancer.* 106:817–820.
3. Ho, W.Y., J.N. Blattman, M.L. Dossett, C. Yee, and P.D. Greenberg. 2003. Adoptive immunotherapy: engineering T cell responses as biologic weapons for tumor mass destruction. *Cancer Cell.* 3:431–437.
4. Sadelain, M., I. Riviere, and R. Brentjens. 2003. Targeting tumours with genetically enhanced T lymphocytes. *Nat. Rev. Cancer.* 3:35–45.
5. Schuler, G., B. Schuler-Thurner, and R.M. Steinman. 2003. The use of dendritic cells in cancer immunotherapy. *Curr. Opin. Immunol.* 15:138–147.
6. Gilboa, E. 2004. The promise of cancer vaccines. *Nat. Rev. Cancer.* 4:401–411.
7. Blattman, J.N., and P.D. Greenberg. 2004. Cancer immunotherapy: a treatment for the masses. *Science.* 305:200–205.
8. Dudley, M.E., and S.A. Rosenberg. 2003. Adoptive-cell-transfer therapy for the treatment of patients with cancer. *Nat. Rev. Cancer.* 3:666–675.
9. Pardoll, D. 2003. Does the immune system see tumors as foreign or self? *Annu. Rev. Immunol.* 21:807–839.
10. Kircher, M.F., J.R. Allport, E.E. Graves, V. Love, L. Josephson, A.H. Lichtman, and R. Weissleder. 2003. In vivo high resolution three-dimensional imaging of antigen-specific cytotoxic T-lymphocyte trafficking to tumors. *Cancer Res.* 63:6838–6846.
11. Mandl, S., C. Schimmelpfennig, M. Edinger, R.S. Negrin, and C.H. Contag. 2002. Understanding immune cell trafficking patterns via in vivo bioluminescence imaging. *J. Cell. Biochem. Suppl.* 39:239–248.
12. Luster, A.D., R. Alon, and U.H. von Andrian. 2005. Immune cell migration in inflammation: present and future therapeutic targets. *Nat. Immunol.* 6:1182–1190.
13. Sallusto, F., and C.R. Mackay. 2004. Chemoattractants and their receptors in homeostasis and inflammation. *Curr. Opin. Immunol.* 16:724–731.
14. Zhang, T., R. Somasundaram, K. Berencsi, L. Caputo, P. Rani, D. Guerry, E. Furth, B.J. Rollins, M. Putt, P. Gimotty, et al. 2005. CXC chemokine ligand 12 (stromal cell-derived factor 1 alpha) and CXCR4-dependent migration of CTLs toward melanoma cells in organotypic culture. *J. Immunol.* 174:5856–5863.
15. Musha, H., H. Ohtani, T. Mizoi, M. Kinouchi, T. Nakayama, K. Shiiba, K. Miyagawa, H. Nagura, O. Yoshie, and I. Sasaki. 2005. Selective infiltration of CCR5(+)CXCR3(+) T lymphocytes in human colorectal carcinoma. *Int. J. Cancer.* 116:949–956.
16. Blankenstein, T. 2005. The role of tumor stroma in the interaction between tumor and immune system. *Curr. Opin. Immunol.* 17:180–186.
17. Spiotto, M.T., D.A. Rowley, and H. Schreiber. 2004. Bystander elimination of antigen loss variants in established tumors. *Nat. Med.* 10:294–298.
18. Rothstein, T.L., M. Mage, G. Jones, and L.L. McHugh. 1978. Cytotoxic T lymphocyte sequential killing of immobilized allogeneic tumor target cells measured by time-lapse microcinematography. *J. Immunol.* 121:1652–1656.
19. Sanderson, C.J. 1976. The mechanism of T cell mediated cytotoxicity. II. Morphological studies of cell death by time-lapse microcinematography. *Proc. R. Soc. Lond. B. Biol. Sci.* 192:241–255.
20. Matter, A. 1979. Microcinematographic and electron microscopic analysis of target cell lysis induced by cytotoxic T lymphocytes. *Immunology.* 36:179–190.
21. Okada, T., M.J. Miller, I. Parker, M.F. Krummel, M. Neighbors, S.B. Hartley, A. O'Garra, M.D. Cahalan, and J.G. Cyster. 2005. Antigen-engaged B cells undergo chemotaxis toward the T zone and form motile conjugates with helper T cells. *PLoS Biol.* 3:e150.
22. Miller, M.J., S.H. Wei, M.D. Cahalan, and I. Parker. 2003. Autonomous T cell trafficking examined in vivo with intravital two-photon microscopy. *Proc. Natl. Acad. Sci. USA.* 100:2604–2609.
23. Germain, R.N., F. Castellino, M. Chieppa, J.G. Egen, A.Y. Huang, L.Y. Koo, and H. Qi. 2005. An extended vision for dynamic high-resolution intravital immune imaging. *Semin. Immunol.* 17:431–441.
24. Cahalan, M.D., I. Parker, S.H. Wei, and M.J. Miller. 2002. Two-photon tissue imaging: seeing the immune system in a fresh light. *Nat. Rev. Immunol.* 2:872–880.
25. Sumen, C., T.R. Mempel, I.B. Mazo, and U.H. von Andrian. 2004. Intravital microscopy: visualizing immunity in context. *Immunity.* 21:315–329.
26. Bousso, P., and E.A. Robey. 2004. Dynamic behavior of T cells and thymocytes in lymphoid organs as revealed by two-photon microscopy. *Immunity.* 21:349–355.
27. Kawakami, N., U.V. Nagerl, F. Odoardi, T. Bonhoeffer, H. Wekerle, and A. Flugel. 2005. Live imaging of effector cell trafficking and autoantigen recognition within the unfolding autoimmune encephalomyelitis lesion. *J. Exp. Med.* 201:1805–1814.
28. Miller, M.J., S.H. Wei, I. Parker, and M.D. Cahalan. 2002. Two-photon imaging of lymphocyte motility and antigen response in intact lymph node. *Science.* 296:1869–1873.
29. Bousso, P., and E. Robey. 2003. Dynamics of CD8+ T cell priming by dendritic cells in intact lymph nodes. *Nat. Immunol.* 4:579–585.
30. Mempel, T.R., S.E. Henrickson, and U.H. Von Andrian. 2004. T-cell priming by dendritic cells in lymph nodes occurs in three distinct phases. *Nature.* 427:154–159.
31. Shakhar, G., R.L. Lindquist, D. Skokos, D. Dudziak, J.H. Huang, M.C. Nussenzweig, and M.L. Dustin. 2005. Stable T cell-dendritic cell interactions precede the development of both tolerance and immunity in vivo. *Nat. Immunol.* 6:707–714.
32. Hugues, S., L. Fetler, L. Bonifaz, J. Helft, F. Amblard, and S. Amigorena. 2004. Distinct T cell dynamics in lymph nodes during the induction of tolerance and immunity. *Nat. Immunol.* 5:1235–1242.
33. Tang, Q., J.Y. Adams, A.J. Tooley, M. Bi, B.T. Fife, P. Serra, P. Santamaria, R.M. Locksley, M.F. Krummel, and J.A. Bluestone. 2006. Visualizing regulatory T cell control of autoimmune responses in nonobese diabetic mice. *Nat. Immunol.* 7:83–92.
34. Zinselmeyer, B.H., J. Dempster, A.M. Gurney, D. Wokosin, M. Miller, H. Ho, O.R. Millington, K.M. Smith, C.M. Rush, I. Parker, et al. 2005. In situ characterization of $CD4^+$ T cell behavior in mucosal and systemic lymphoid tissues during the induction of oral priming and tolerance. *J. Exp. Med.* 201:1815–1823.
35. Sawada, S., J.D. Scarborough, N. Killeen, and D.R. Littman. 1994. A lineage-specific transcriptional silencer regulates CD4 gene expression during T lymphocyte development. *Cell.* 77:917–929.
36. Wurster, A.L., G. Siu, J.M. Leiden, and S.M. Hedrick. 1994. Elf-1 binds to a critical element in a second CD4 enhancer. *Mol. Cell. Biol.* 14:6452–6463.
37. Kowalczyk, D.W., A.P. Wlazlo, M. Blaszczyk-Thurin, Z.Q. Xiang, W. Giles-Davis, and H.C. Ertl. 2001. A method that allows easy characterization of tumor-infiltrating lymphocytes. *J. Immunol. Methods.* 253:163–175.
38. Haas, A.R., J. Sun, A. Vachani, A.F. Wallace, M. Silverberg, V. Kapoor, and S.M. Albelda. 2006. Cycloxygenase-2 inhibition augments the efficacy of a cancer vaccine. *Clin. Cancer Res.* 12:214–222.
39. Condeelis, J., and J.E. Segall. 2003. Intravital imaging of cell movement in tumours. *Nat. Rev. Cancer.* 3:921–930.
40. Underhill, D.M., M. Bassetti, A. Rudensky, and A. Aderem. 1999. Dynamic interactions of macrophages with T cells during antigen presentation. *J. Exp. Med.* 190:1909–1914.
41. Witt, C.M., S. Raychaudhuri, B. Schaefer, A.K. Chakraborty, and E.A. Robey. 2005. Directed migration of positively selected thymocytes visualized in real time. *PLoS Biol.* 3:e160.
42. Friedl, P., S. Borgmann, and E.B. Brocker. 2001. Amoeboid leukocyte crawling through extracellular matrix: lessons from the Dictyostelium paradigm of cell movement. *J. Leukoc. Biol.* 70:491–509.
43. Bromley, S.K., W.R. Burack, K.G. Johnson, K. Somersalo, T.N. Sims, C. Sumen, M.M. Davis, A.S. Shaw, P.M. Allen, and M.L. Dustin. 2001. The immunological synapse. *Annu. Rev. Immunol.* 19:375–396.
44. McGavern, D.B., U. Christen, and M.B. Oldstone. 2002. Molecular anatomy of antigen-specific CD8(+) T cell engagement and synapse formation in vivo. *Nat. Immunol.* 3:918–925.
45. Gunzer, M., A. Schafer, S. Borgmann, S. Grabbe, K.S. Zanker, E.B. Brocker, E. Kampgen, and P. Friedl. 2000. Antigen presentation in extracellular matrix: interactions of T cells with dendritic cells are dynamic, short lived, and sequential. *Immunity.* 13:323–332.
46. Bingle, L., N.J. Brown, and C.E. Lewis. 2002. The role of tumour-associated macrophages in tumour progression: implications for new anticancer therapies. *J. Pathol.* 196:254–265.

47. Huse, M., B.F. Lillemeier, M.S. Kuhns, D.S. Chen, and M.M. Davis. 2006. T cells use two directionally distinct pathways for cytokine secretion. *Nat. Immunol.* 7:247–255.
48. Mora, J.R., M.R. Bono, N. Manjunath, W. Weninger, L.L. Cavanagh, M. Rosemblatt, and U.H. Von Andrian. 2003. Selective imprinting of gut-homing T cells by Peyer's patch dendritic cells. *Nature*. 424: 88–93.
49. Pearce, E.L., A.C. Mullen, G.A. Martins, C.M. Krawczyk, A.S. Hutchins, V.P. Zediak, M. Banica, C.B. DiCioccio, D.A. Gross, C.A. Mao, et al. 2003. Control of effector CD8+ T cell function by the transcription factor Eomesodermin. *Science*. 302:1041–1043.
50. Mrass, P., M. Rendl, M. Mildner, F. Gruber, B. Lengauer, C. Ballaun, L. Eckhart, and E. Tschachler. 2004. Retinoic acid increases the expression of p53 and proapoptotic caspases and sensitizes keratinocytes to apoptosis: a possible explanation for tumor preventive action of retinoids. *Cancer Res.* 64:6542–6548.
51. von Andrian, U.H. 1996. Intravital microscopy of the peripheral lymph node microcirculation in mice. *Microcirculation*. 3:287–300.